J. Fluid Mech. (1995), *vol.* 295, *pp.* 247–261

Simultaneous sedimentation and coalescence of a dilute dispersion of small drops

By HUA WANG† AND ROBERT H. DAVIS‡
Department of Chemical Engineering, University of Colorado, Boulder, CO 80309-0424, USA

(Received 17 November 1993 and in revised form 16 February 1995)

Macroscopic phase separation and the evolution of the drop size distribution for non-homogeneous dispersions, in which buoyancy-driven settling and coalescence of drops cause spatial as well as temporal variations of the drop size distribution, was analysed by numerical solution of the population dynamics equations. Collision efficiencies based on detailed hydrodynamic interactions of spherical drops with clean interfaces were incorporated in the description of the pairwise drop coalescence rates. A dimensionless parameter that characterizes the relative importance of settling and coalescence was identified. For finite values of this parameter, the phase separation rates and average drop size initially increase owing to coalescence, and then decrease owing to the larger drops settling out of the dispersion.

1. Introduction

Dispersions of drops of one fluid in a second, immiscible fluid are frequently encountered in industrial and natural processes such as extraction, raindrop growth, food and beverage processing, and the formation of liquid-phase-miscibility-gap materials. In a finite container, drop migration due to buoyancy forces generally results in an inhomogeneous dispersion with phase separation. In certain applications, this is the desired result. An example is aqueous biphasic partitioning, in which the two phases must separate subsequent to mixing for the partitioned component to be recovered. A counter-example is the processing of liquid-phase-miscibility-gap metals, for which the desired product is a composite material with fine particles of one metal uniformly dispersed in a matrix of the other. In this paper, we predict the macroscopic phase separation and the temporal and spatial evolution of the drop size distribution for small drops in a dilute finite dispersion subject to gravitational motion and coalescence.

Gravity sedimentation of particles in the absence of coalescence or aggregation has been studied extensively (e.g. Davis & Acrivos 1985). Similarly, coalescence of drops in spatially uniform dispersions in the absence of phase separation has been modelled extensively (Berry & Reinhardt 1974; Rogers & Davis 1990*a*, *b*; Satrape 1992; Wang & Davis 1993; Zhang, Wang & Davis 1993). However, there are only a few studies of simultaneous sedimentation and coalescence. A notable example is the important study of Reddy, Melik & Fogler (1981). They developed a general population dynamics equation which accounts for creaming (sedimentation) as well as flocculation (coalescence) due to Brownian motion and gravity sedimentation. Example numerical calculations were done for a specific oil-in-water system. They noted that the size distribution shifts toward larger particles (drops) when flocculation dominates, toward

† Present address: Department of Chemical Engineering, MIT, Cambridge, MA 02139, USA.
‡ To whom correspondence should be addressed.

smaller particles when creaming dominates, and initially toward larger particles and subsequently toward small particles when both mechanisms are important.

In the current work, we predict the macroscopic phase separation and drop size distributions for buoyancy-driven sedimentation and coalescence of immiscible dispersions of drops by solving the general population dynamics equations with both temporal and spatial dependence retained, and incorporating a mass balance on the drops arriving at the moving interface between the two phases which form. The problem is similar to that considered by Reddy *et al.* (1981), except that the rate of phase separation is specifically addressed in our work. Also, complete hydrodynamic interactions between pairs of spherical drops with internal circulation are accounted for by using the droplet collision efficiencies recently computed by Zhang & Davis (1991), whereas Reddy *et al.* (1981) employed sedimentation velocities for rigid spheres and used collision efficiencies based on Brownian aggregation of rigid particles. Thus, the current work applies to drops with clean interfaces, whereas the previous work applies to drops which are either extremely viscous or else have surfactants present which retard interfacial motion and internal circulation. Colloidal phenomena such as Brownian motion and electrostatic repulsion were considered by Reddy *et al.* (1981), but we restrict our attention to larger drops for which these effects are small.

It is assumed in this study that the drops are sufficiently small that both the Reynolds number and capillary number are small compared to unity, indicating that inertia is negligible and that the drops remain spherical, but that the drops are not so small that Brownian motion is significant. For common liquids, these conditions are met for drops with diameters of 2–100 μm (Zhang & Davis 1991). In §2, the problem to be solved is defined, and the population dynamics models and the expression for collision rate are presented. In §3, a dimensionless parameter characterizing the relative importance of coalescence and settling is identified, and the method of solution of the general population dynamics equations is discussed. In §4, the results of numerical modelling of phase separation and the evolution of drop size distribution are presented and discussed. Most of the results are presented in dimensionless form, with an exception made for illustrative purposes for a typical dispersion. Concluding remarks are given in §5.

2. Theoretical development

We consider a dilute dispersion of spherical drops of viscosity μ' and density ρ' dispersed in an immiscible fluid of viscosity μ and density ρ. Both fluids are Newtonian, and it is assumed that there are no surfactants on the drop surfaces. The typical problem of interest is illustrated in figure 1. The initial condition (figure 1*a*) is a uniform suspension of droplets or bubbles of one fluid dispersed in a second, immiscible fluid. After mixing is stopped, the drops (or bubbles) begin to rise owing to buoyancy (assuming, for illustrative purposes, that $\rho' < \rho$). It is assumed that there is no imposed flow after stirring ceases, other than as a result of the motion of individual drops. As the drops reach the top of the container, they coalesce into an overlying, segregated layer of the dispersed-phase fluid (figure 1*b*). This layer grows with time (figure 1*c*) until all of the dispersed drops have coalesced into it (figure 1*d*). The problem is complicated by the possibility that the drops also collide and coalesce with each other as they rise, and, because the larger drops move faster and leave the smaller ones behind, the drop size distribution varies with both time and position.

The temporal and spatial evolutions of the drop size distribution during a phase separation process, such as illustrated in figure 1, are studied by using population

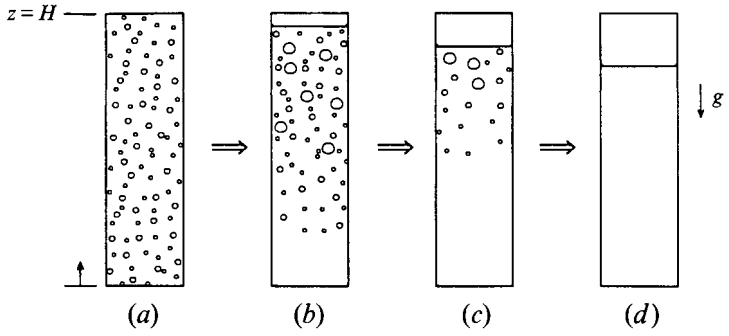

FIGURE 1. Schematic of the time evolution of the phase separation process due to the simultaneous migration and coalescence of rising drops or bubbles.

dynamics equations. In discretized form, these equations are given by a differential mass balance on each size category, i:

$$\frac{\partial n_i}{\partial t}+\frac{\partial(u_i n_i)}{\partial z}=\frac{1}{2}\sum_{j=1}^{i-1} J_{j(i-j)}-\sum_{j=1}^{N} J_{ij}, \quad i=1,2,\ldots,N, \tag{1}$$

where n_i is the number of drops per unit volume in the discrete size category i, u_i is the settling velocity of drops of size i, t is time, z is the direction of drop migration (vertical, as defined in figure 1), J_{ij} is the rate of collisions per unit volume of size-i drops with size-j drops, and N is the total number of size categories. The first term on the right-hand side of (1) is the rate of formation of size-i drops by collision of two smaller drops, where the factor of $\frac{1}{2}$ avoids double counting, and the second term is the rate of loss of size-i drops due to their collisions to form larger drops.

The collision rate between drops in size category i (larger drops) and the size category j (smaller drops) may be expressed as (Zhang & Davis 1991)

$$J_{ij}=n_i n_j \pi(a_i+a_j)^2 \,|u_i-u_j|\, E_{ij}, \tag{2}$$

where a_i and a_j are the large and small drop radii, respectively, and E_{ij} is the collision efficiency. The collision efficiency equals unity when the drops move independently until colliding; values of E_{ij} differing from unity take account of the hydrodynamic and repulsive forces which cause the drops to move around one another and the attractive forces which pull them together. In general, E_{ij} is a function of the radius ratio, $\lambda=a_j/a_i$, the viscosity ratio, $\hat{\mu}=\mu'/\mu$, and any dimensionless measures of the magnitude of the interparticle forces between the drops in the system of interest. The collision efficiencies computed by Zhang & Davis (1991) account for the possibility of attractive van der Waals forces but not for repulsive electrostatic forces. It is assumed that collisions result in coalescence rather than in the two drops bouncing off each other or in the formed drop subsequently breaking into smaller drops. This assumption is expected to be valid in the absence of stirring, turbulence, and inertia, which might cause drop breakage.

The speed of a single drop due to gravity sedimentation was first analysed independently by Hadamard (1911) and Rybczynski (1911):

$$u_i=\frac{2(\hat{\mu}+1)(\rho'-\rho)a_i^2 g}{3(3\hat{\mu}+2)\mu}, \tag{3}$$

where g is the gravitational acceleration. This expression is valid provided that the Reynolds number, $Re=\rho u_i a_i/\mu$, is small compared to unity. In a dispersion of drops,

the average sedimentation velocity is given by (3) multiplied by a hindered settling function which accounts for the effects of multidroplet interactions and fluid backflow. For the dilute dispersions considered here, these effects are negligible.

The initial condition for (1) for well-mixed dispersions is

$$n_i = n_{io}, \quad t = 0, \quad 0 \leqslant z \leqslant H, \quad i = 1, 2, \ldots, N. \tag{4}$$

The rate at which the lighter phase grows at the top of the vessel due to droplets reaching this phase is determined by a mass balance:

$$-A\frac{\mathrm{d}h_u}{\mathrm{d}t} = \sum_{i=1}^{N} A\left(u_i - \frac{\mathrm{d}h_u}{\mathrm{d}t}\right) n_i v_i,$$

where the left-hand side is the rate of accumulation of the upper phase and the right-hand side is the flux of drops into the upper phase, or

$$\frac{\mathrm{d}h_u}{\mathrm{d}t} = -\sum_{i=1}^{N} u_i n_i v_i/(1-\phi) \quad \text{at} \quad z = h_u(t), \tag{5}$$

where A is the cross-sectional area of the container, $v_i = \frac{4}{3}\pi a_i^3$ is the volume of a drop of size i, and $\phi = \Sigma_{i=1}^{N} v_i n_i$ is the total volume fraction of droplets in the suspension just below the upper interface at $z = h_u(t)$. The initial condition is $h_u = H$ at $t = 0$.

3. Method of solution

We define the following dimensionless variables: $\hat{a}_i = a_i/a_o$, $\hat{z} = z/H$, $\hat{u}_i = u_i/u_o$, $\hat{t} = tu_o/H$, and $\hat{n}_i = n_i 4\pi a_o^3/3\phi_o$, where a_o is a characteristic drop radius, defined here as the average radius in the initial distribution, u_o is the characteristic gravity settling velocity of isolated drops with radius a_o, and ϕ_o is the initial volume fraction of the dispersed drops. In dimensionless form, (1), together with (2), becomes

$$\frac{\partial \hat{n}_i}{\partial \hat{t}} + \frac{\partial(\hat{u}_i \hat{n}_i)}{\partial \hat{z}} = \frac{1}{2}\left(\frac{3\phi_o H}{4a_o}\right)\sum_{j=1}^{i-1} \hat{n}_j \hat{n}_{i-j}(\hat{a}_j + \hat{a}_{i-j})^2 \,|\, \hat{u}_{i-j} - \hat{u}_j \,|\, E_{i-j,j}$$

$$+ \left(\frac{3\phi_o H}{4a_o}\right)\sum_{i=1}^{N} \hat{n}_i \hat{n}_j (\hat{a}_i + \hat{a}_j)^2 \,|\, \hat{u}_i - \hat{u}_j \,|\, E_{i,j}, \quad i = 1, 2, \ldots, N. \tag{6}$$

Note that the relative importance of coalescence and sedimentation depends on a single parameter, $N_\tau \equiv \tau_s/\tau_c = 3\phi_o H/4a_o$, where $\tau_s = H/u_o$ is the characteristic settling time for a drop with velocity u_o and radius a_o to travel the length of the container, and $\tau_c = 4a_o/(3\phi_o u_o)$ is the characteristic coalescence time for drops having characteristic radius a_o, velocity u_o, and an initial total volume fraction of ϕ_o (Wang & Davis 1993). N_τ is roughly the number of collisions occurring for a drop with radius a_o as it travels the length of the container, although we note that the collision frequency may be much lower if the collision efficiencies are much less than unity. When $N_\tau \ll 1$, the right-hand side of (6) is small, and so coalescence is negligible, and the two terms on the left-hand side balance. In contrast, coalescence is expected to be rapid when $N_\tau \gg 1$. The right-hand side of (6) is then balanced primarily by the time-dependent term and the coalescence process is quasi-homogeneous.

The dimensionless version of (5) is

$$\frac{\mathrm{d}\hat{h}_u}{\mathrm{d}\hat{t}} = -\frac{\phi_o}{1-\phi}\sum_{i=1}^{N} \hat{u}_i \hat{n}_i \quad \text{at} \quad \hat{z} = \hat{h}_u. \tag{7}$$

The initial size distributions, assumed uniform for $0 \leqslant \hat{z} \leqslant 1$, were chosen to be normal distributions on a number basis, as specified by the number-averaged drop radius, a_o, and the standard deviation, σ, of drop radii. In dimensionless form, normal distributions are characterized by a single dimensionless parameter, $\hat{\sigma} = \sigma/a_o$. Although initial distributions are typically specified in terms of the number distribution of the drops, the common practice (Rogers & Davis 1990*a*; Satrape 1992; Wang & Davis 1993; Zhang *et al.* 1993) is to follow the evolution of the size distribution in terms of a volume density function, $f(\ln \hat{a})$, defined such that $f(\ln \hat{a})\, \mathrm{d} \ln \hat{a}$ is the volume of droplets having dimensionless radii whose natural logarithm is within the interval $\ln \hat{a} \pm \frac{1}{2} \mathrm{d} \ln \hat{a}$, per unit volume of dispersion. Thus, the integral of $f(\ln \hat{a})$ equals the total volume fraction of the dispersed phase:

$$\int_0^\infty f(\ln \hat{a})\, \mathrm{d} \ln \hat{a} = \phi(\hat{z}, \hat{t}), \tag{8}$$

where $\phi(\hat{z}, \hat{t})$ is the total volume fraction of the dispersed phase at given position $\hat{z}$ and time $\hat{t}$.

The population dynamics equations were solved using the hybrid numerical scheme used previously by Clark (1973), Clark & Hall (1979), and Hall (1980) in atmospheric modelling of cloud and raindrop formation. This scheme is a combination of the Lax–Wendroff finite-difference method (Lax & Wendroff 1960; Fletcher 1991), or the Crowley method (Crowley 1968), which is equivalent to Lax–Wendroff method for the conditions in this study, and a first-order upstream difference method. Such a hybrid scheme assures the positive definiteness of the positive variable, $\hat{n}_i$, and does not have the severe numerical dispersion properties common to the upstream-difference method. Interested readers are referred to Hall (1980) for a detailed discussion of the method.

The numerical method used logarithmic discretization of drop spectra into N categories which have equal spacing in the logarithm of droplet mass or volume, with the mass or volume of a droplet within each discrete category doubling every fourth category, as described by Rogers & Davis (1990*a*) and Wang & Davis (1993). The range of dimensionless droplet radii considered is 0.01 to 100, although the numerical implementation can handle even larger size ranges. The container is divided into 50 equal-spaced segments, so that the spatial step size is $\Delta\hat{z} = 0.02$. The dimensionless time step $\Delta\hat{t}$ used in the calculations is typically $\Delta\hat{t} = 10^{-5}$–10^{-3}, depending on the parameter N_τ, in order to meet the stability criterion $\hat{u}\Delta\hat{t}/\Delta\hat{z} \leqslant 1$ for the Lax–Wendroff numerical scheme. The step sizes in space, time, and radius were chosen based on halving their values until the calculated average radius of the distribution converged within 2%. The total volume fraction of the dispersed phase was computed after each time step and checked against the input value ϕ_o; the agreement was within 5% for the conditions used in this study. As a further check of the calculations, the collision kernals of Reddy *et al.* (1981) were used in our numerical scheme. The average radii for various times were found to agree with those extracted from the distribution graphs of Reddy *et al.* (1981) to within 1–5%.

4. Results and discussion

The dimensionless parameters which affect the macroscopic behaviour of a dispersion include the time-scale ratio, N_τ, the viscosity ratio, $\hat{\mu} = \mu'/\mu$, the dimensionless standard deviation of radii in the initial distribution, $\hat{\sigma} = \sigma/a_o$, and the initial volume fraction, ϕ_o. Note that the value of ϕ_o affects the dimensionless rate of phase separation through (7), but it is scaled out of the population dynamics equation

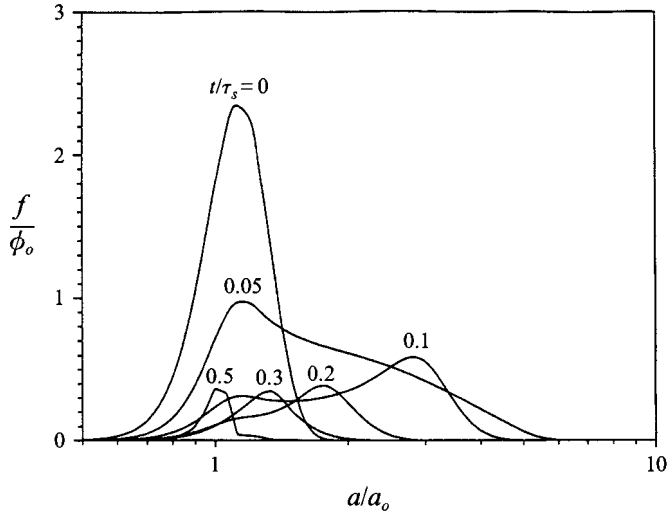

FIGURE 2. Time evolution of the drop size distribution at $\hat{z} = 0.5$ for a dispersion having $\hat{\mu} = 0.1$, $\hat{\sigma} = 0.2$, and $N_\tau = 50$.

(6) which governs the size distribution. Although $\hat{\mu}$ does not appear explicitly in the dimensionless equations, it does appear implicitly because the collision efficiencies decrease with increasing $\hat{\mu}$ (Zhang & Davis 1991). In order to reduce the number of parameters, we consider dispersions for which interparticle forces are negligible, except that van der Waals attractions are included in the physical example provided at the end of this section.

When the characteristic coalescence time for a dispersion is much larger than the characteristic sedimentation time scale, so that $N_\tau \to 0$, the drops settle out of the dispersion with no collisions and coalescence. In this limit, the population dynamics equation (6) simplifies to

$$\frac{\partial \hat{n}_i}{\partial \hat{t}} + \frac{\partial (\hat{u}_i \hat{n}_i)}{\partial \hat{z}} = 0, \quad i = 1, 2, \ldots, N. \tag{9}$$

Using the method of characteristics, (9) has the analytical solution

$$\hat{n}_i(\hat{z}, \hat{t} + \Delta\hat{t}) = \hat{n}_i(\hat{z} - \hat{u}_i \Delta\hat{t}, \hat{t}), \quad i = 1, 2, \ldots, N. \tag{10}$$

The above solution indicates that all drops with velocity $\hat{u}_i$ located at the position $\hat{z} - \hat{u}_i \Delta\hat{t}$ will be located at the position $\hat{z}$ after $\Delta\hat{t}$ has elapsed.

When the characteristic coalescence time for a dispersion is much less than the characteristic sedimentation time scale, so that $N_\tau \to \infty$, then coalescence is the dominant process. In this limit, corresponding to an infinite container, the dispersion will be spatially homogeneous. Note that spatial inhomogeneities also do not develop in the interior of a finite container for short times, because drops which sediment out of a control volume are replaced at an equal rate by drops moving into the control volume. The evolution of the drop size distribution due to gravitational collisions for homogeneous dispersions has been studied in detail by Wang & Davis (1993).

In figure 2, we show typical plots of the droplet size distribution evolution at the middle of the container, $\hat{z} = 0.5$, due to simultaneous sedimentation and coalescence for a dispersion system with $\hat{\mu} = 0.1$, $\hat{\sigma} = 0.2$, and $N_\tau = 50$. It is shown that the drop size distribution initially shifts to large drop sizes due to coalescence. After a certain

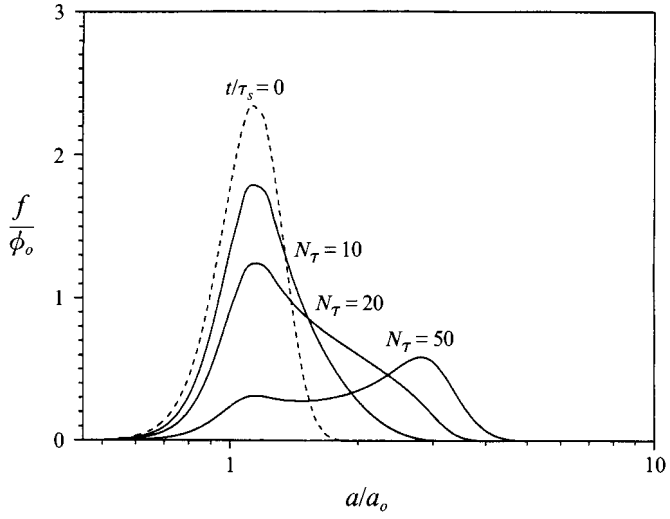

FIGURE 3. Time evolution of the drop size distribution at $\hat{z} = 0.5$ and $t/\tau_s = 0.1$, for a dispersion having $\hat{\mu} = 0.1$, $\hat{\sigma} = 0.2$ and different N_τ; the dotted line represents the initial distribution at $t/\tau_s = 0$.

time, however, the drop size distribution begins to shift toward small drop sizes, owing to the larger drops settling out of the dispersion. It is also shown in figure 2 that the areas under the curves become smaller with time increasing, corresponding to decreasing volume fraction at $\hat{z} = 0.5$. Similar behaviour of the evolution of the drop size distribution has been predicted by Reddy *et al.* (1981). It is noted that this behaviour is significantly different from the evolution of the drop size distribution with $N_\tau = 0$ (no coalescence) or $N_\tau = \infty$ (homogeneous dispersions). When coalescence is absent, the drop size distribution shifts monotonically toward smaller drops, as the large drops settle out. In the case of homogeneous dispersions, the drop size shifts monotonically toward larger drops owing to coalescence, and the drop size distribution evolves into a bimodal distribution with large spread (Wang & Davis 1993).

The influence of the time-scale ratio N_τ on the evolution of drop size distribution at dimensionless position $\hat{z} = 0.5$ and dimensionless time $t/\tau_s = 0.1$ is shown in figure 3 for a dispersion with $\hat{\sigma} = 0.2$, and $\hat{\mu} = 0.1$. It is apparent that increasing N_τ corresponds to increasing the relative importance of coalescence; thus, the average drop size increases with N_τ increasing. Referring to the definition $N_\tau = 3\phi_o H/4a_o$, increasing values of this parameter occur for increasing concentration and increasing container height divided by the average radii; both effects allow more collisions. Figure 4 shows the corresponding results for the evolution of the average radius (defined in Wang & Davis 1993 as the radius of a drop having the mass-averaged volume) versus time for different values of N_τ. It is seen that the average droplet radius initially increases with time owing to coalescence; after the larger drops sediment out of the dispersion, the average radius begin to decrease. The maximum average drop radii are $1.43a_o$, $1.74a_o$, and $2.69a_o$, occurring at $t/\tau_s = 0.14$, 0.11 and 0.07, for $N_\tau = 10$, 20 and 50, respectively.

Figure 5 presents results of the evolution of the average radius versus time at different positions for a dispersion having $\hat{\mu} = 0.1$, $\hat{\sigma} = 0.2$ and $N_\tau = 50$. It is seen that the drop growth rates for short times are the same for all three positions; this is a result of the dispersion remaining homogeneous until the largest drops rise past a given position. At $t/\tau_s \doteq 0.04$, however, the average radius at $\hat{z} = 0.1$ begins to decrease,

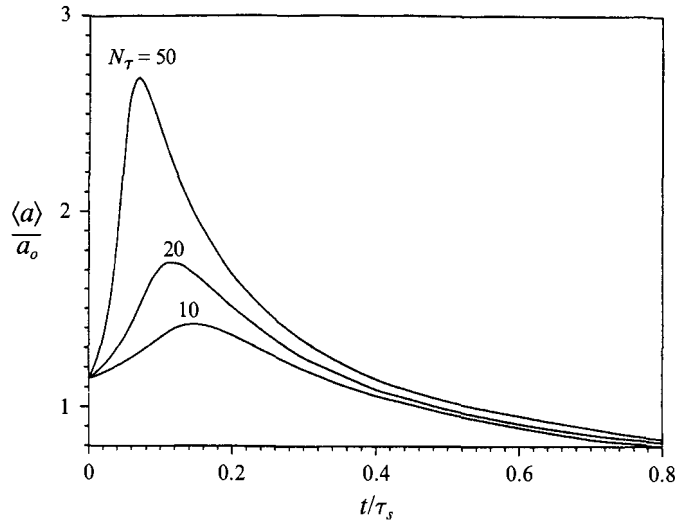

FIGURE 4. Time evolution of the average drop radius at $\hat{z} = 0.5$ for a dispersion having $\hat{\mu} = 0.1$ and $\hat{\sigma} = 0.2$.

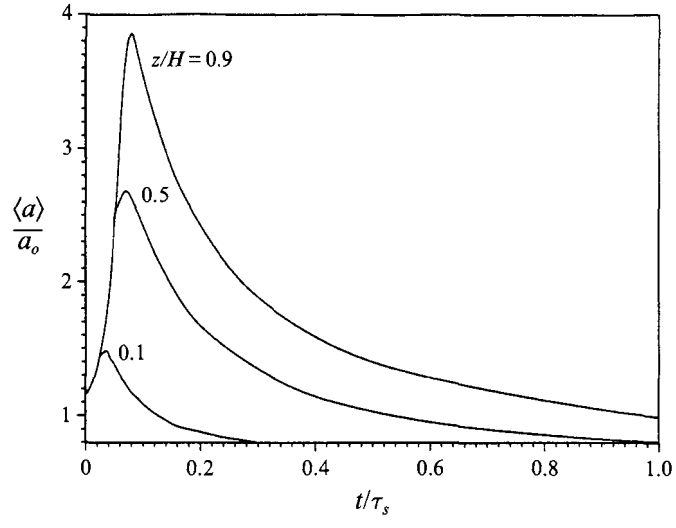

FIGURE 5. The evolution of the average drop radius with time at different positions for a dispersion having $\hat{\mu} = 0.1$, $\hat{\sigma} = 0.2$, and $N_\tau = 50$.

while the average drop radii at $\hat{z} = 0.5$ and 0.9 continue to increase with time. The times for the average radii to reach their maxima of $1.48a_o$, $2.78a_o$, and $3.86a_o$ are $0.04t/\tau_s$, $0.07t/\tau_s$, and $0.08t/\tau_s$, for $\hat{z} = 0.1$, 0.5 and 0.9, respectively. Figure 6 shows the corresponding drop size distributions for different positions at dimensionless time $t/\tau_s = 0.1$ for the same dispersion as in figure 5. The greatest shifts toward larger drops occur near the top of the container, because the rising drops experience more collisions as they travel further to reach the upper regions of the container. At dimensionless time $t/\tau_s = 0.1$, most of the large drops have floated out of the part of dispersion with $\hat{z} \leqslant 0.1$; thus, the volume fraction at $\hat{z} = 0.1$ at $t/\tau_s = 0.1$, as shown by the area under the curve, is much smaller than that in the initial distribution.

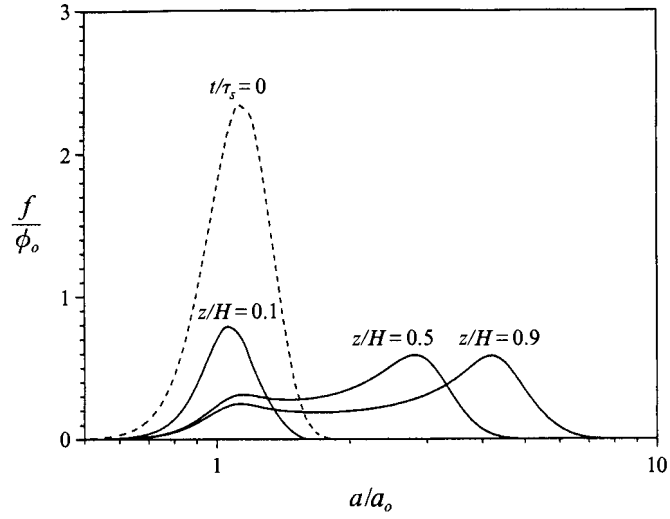

FIGURE 6. The drop size distribution at time $t/\tau_s = 0.1$ and different positions for a dispersion having $\hat{\mu} = 0.1$, $\hat{\sigma} = 0.2$ and $N_\tau = 50$.

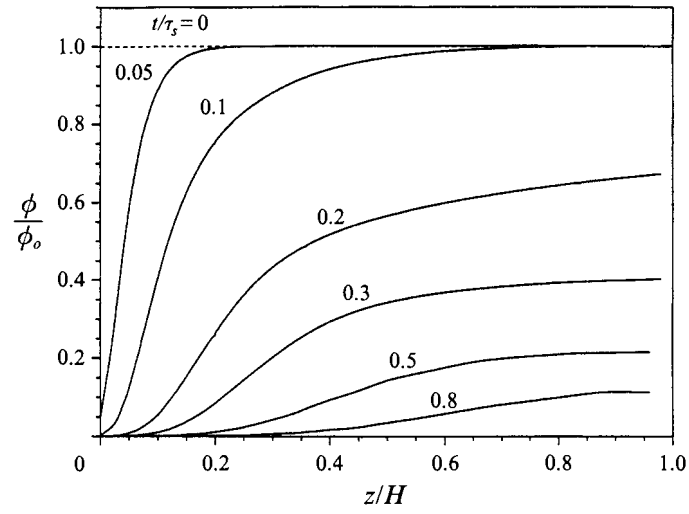

FIGURE 7. The variation of volume fraction with position at different times for a dispersion having $\hat{\mu} = 0.1$, $\hat{\sigma} = 0.2$ and $N_\tau = 20$.

The variation of the droplet volume fraction with dimensionless position $\hat{z}$ at different times is shown in figure 7 for a dispersion with $\hat{\mu} = 0.1$, $\hat{\sigma} = 0.2$, and $N_\tau = 20$. The volume fraction in the lower regions of the container decreases rapidly with time as the drops rise. For short times, the volume fraction in the upper regions of the dispersion is the same as the initial volume fraction. This is because droplets which rise out of a control volume at the top of dispersion are replaced at an equal rate by droplets moving into the control volume. Thus, for short times, the evolution of the drop size distribution in the upper regions of the dispersion will be the same as that predicted for an homogeneous dispersion. With time increasing, however, larger drops rise out of the dispersion, and the volume fraction at any height in the dispersion system is significantly less than the initial volume fraction.

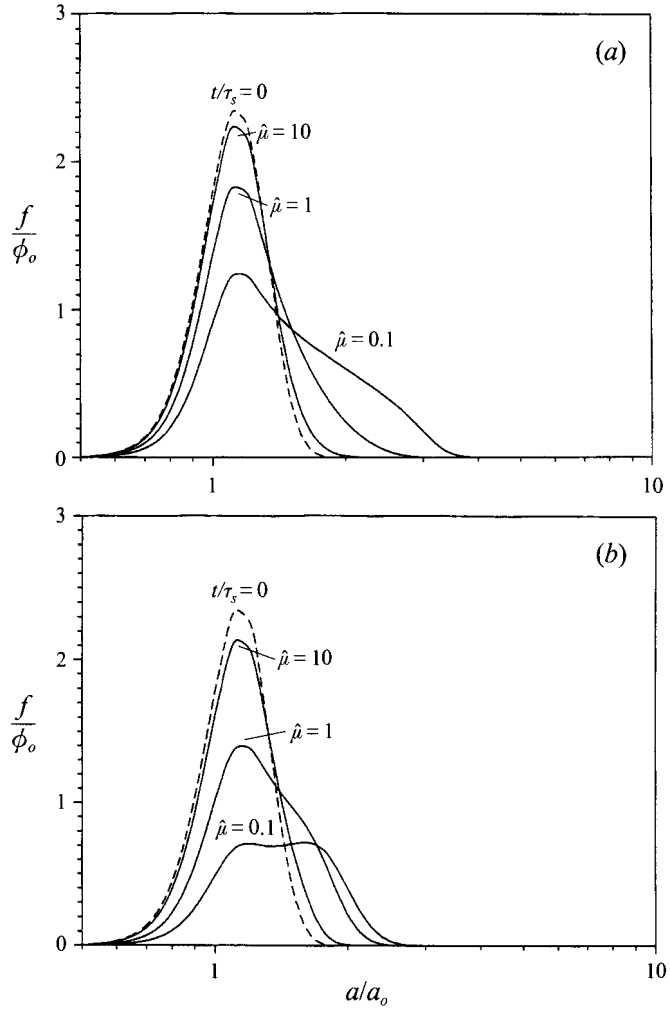

FIGURE 8. The drop size distribution at $\hat{z} = 0.5$ for (*a*) $t/\tau_s = 0.1$ and (*b*) $t/\tau_s = 0.2$, for a dispersion having $\hat{\sigma} = 0.2$ and $N_\tau = 20$; the dotted line for each case is the initial distribution.

Figure 8 represents results of the influence of the viscosity ratio on the evolution of the drop size distribution at dimensionless height $\hat{h} = 0.5$, and dimensionless times $t/\tau_s = 0.1$ and 0.2, for a dispersion having $\hat{\sigma} = 0.2$ and $N_\tau = 20$. It is seen in figure 8(*a*) that, with an increase in the viscosity ratio, the rate of growth of the drop size distribution decreases. For $\hat{\mu} = 0.1$, the drop size distribution shifts significantly toward large drop sizes, while the change of drop size distribution at $t/\tau_s = 0.1$ is insignificant for $\hat{\mu} = 10$. This is because the hydrodynamic resistance between colliding drops increases with an increase in viscosity ratio, leading to very small collision efficiencies for large viscosity ratios. Davis, Schonberg & Rallison (1989) used lubrication theory to describe how the increased internal flow with decreasing drop viscosity allows the surrounding fluid to more easily flow out of the gap separating two colliding drops. As shown by Zhang & Davis (1991), the resulting typical collision efficiencies for gravity-induced coalescence are $O(10^{-1})$ and $O(10^{-2})$, for $\hat{\mu} = 0.1$ and $\hat{\mu} = 10$, respectively. Figure 8(*b*) shows the drop size distribution for the same dispersion at dimensionless time $t/\tau_s = 0.2$. At this time, a significant amount of the

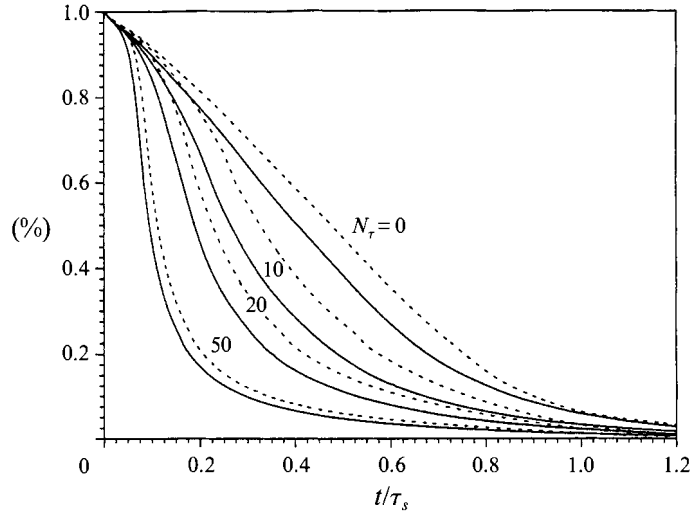

FIGURE 9. Percentage of the mass (or volume) of the dispersed-phase fluid which remains dispersed versus time for a dispersion having $\hat{\mu} = 0.1$, $\phi_o = 0.05$, $\hat{\sigma} = 0.2$ (solid lines), $\hat{\sigma} = 0.1$ (dashed lines) and different N_τ.

drop phase has floated out of the dispersion. Since the drop collision and coalescence rates increase with a decrease in viscosity ratio, and since coalescence results in larger drops which rise out of the dispersion faster, the drop volume fraction at $t/\tau_s = 0.2$ and $\hat{z} = 0.5$, as indicated by the area under each curve, decreases from $0.97\phi_o$ to $0.84\phi_o$ to $0.57\phi_o$ with $\hat{\mu}$ decreasing from 10 to 1 to 0.1.

Figure 9 shows the percentage of volume (or mass) of the dispersed-phase fluid remaining dispersed as a function of time for a dispersion with $\hat{\mu} = 0.1$, $\phi_o = 0.05$, and different N_τ. The solid and dashed lines represent the results for $\hat{\sigma} = 0.2$ and $\hat{\sigma} = 0.1$, respectively. It is seen that increasing the parameter N_τ significantly increases the phase separation process. The times required for 10% of the dispersed-phase fluid to float out of the dispersion (i.e. 90% of drop phase still in the dispersion) for $\hat{\sigma} = 0.2$ are $t/\tau_s = 0.10$, 0.09, 0.08 and 0.05, for $N_\tau = 0$, 10, 20 and 50, respectively. The times required for 90% of the dispersed-phase fluid to float out of the dispersion for $\hat{\sigma} = 0.2$ are $t/\tau_s = 0.86$, 0.67, 0.53 and 0.29, for $N_\tau = 0$, 10, 20 and 50, respectively. Figure 9 also presents results for the influence of the spread of the initial drop size distribution on the phase separation process. It is shown that the phase separation process slows down with $\hat{\sigma}$ decreasing. A smaller spread in the initial distribution implies that the relative velocities of drops in many of the interacting size categories are smaller. Therefore, a lower rate of collisions and phase separation is observed.

Typical results for the gravitational phase separation rate are shown in figure 10 for a dispersion having $\hat{\mu} = 0.1$, $\hat{\sigma} = 0.1$ (dashed lines), $\hat{\sigma} = 0.2$ (solid lines), $\phi_o = 0.05$, and different N_τ. When $N_\tau = 0$, no coalescence occurs. Phase separation then occurs at a constant rate until the largest drops rise out of the dispersion, after which the phase separation rate monotonically decreases owing to fewer and smaller drops arriving at the phase interface. When $N_\tau > 0$, the phase separation rate initially increases, because coalescence leads to larger drops with faster rise rates. Once these drops rise out of suspension, however, the phase separation rate reaches a maximum and then decreases as only smaller drops remain. Note that relatively large values of $N_\tau \geqslant O(10)$ are necessary for coalescence to significantly affect the phase separation process. This is

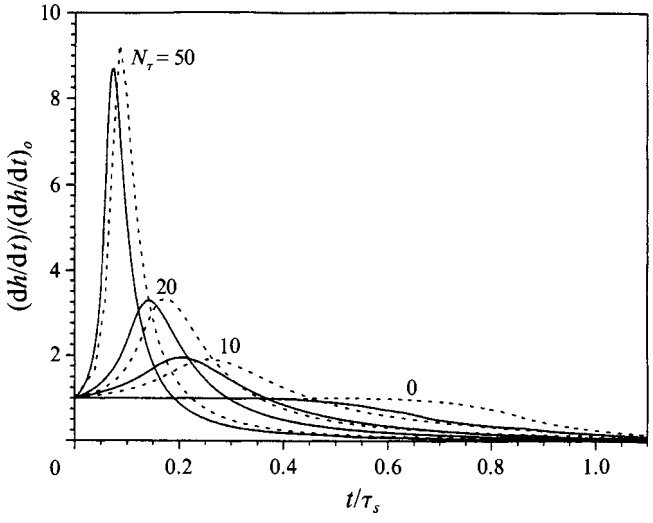

FIGURE 10. The rate of phase separation versus time for a dispersion having $\hat{\mu} = 0.1$, $\hat{\sigma} = 0.2$ (solid lines), $\hat{\sigma} = 0.1$ (dashed lines), $\phi_o = 0.05$ and different N_τ in a container of finite depth.

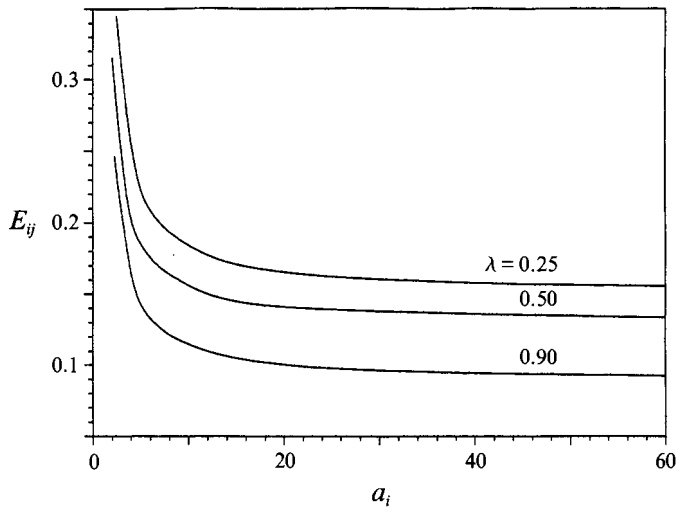

FIGURE 11. The collision efficiency as a function of the radius of the larger drop for lead drops in an aluminium melt at different drop size ratios. The large increases as the drops become small are due to van der Waals attractions.

because typical collision efficiencies are $O(10^{-1})$ for dispersions with $\hat{\mu} = 0.1$ (Zhang & Davis 1991).

Results for a model system

Predictions of the phase separation due to simultaneous sedimentation and coalescence are made for a liquid-phase-miscibility-gap system composed of lead drops in an aluminium melt. This system is of practical use in the formation of self-lubricating bearings. The relative properties of this system at 700 °C are (Smithells 1962; Parsegian & Weiss 1982) $\mu = 1.54 \times 10^{-3}$ kg m^{-1} s^{-1}, $\hat{\mu} = 0.62$, $\gamma = 0.126$ N m^{-1}, $\rho' = 1.02 \times 10^4$ kg m^{-3}, $\rho = 0.24 \times 10^4$ kg m^{-3}, and $A = 10^{-19}$ J, where γ is the interfacial tension and A is the composite Hamaker constant. Since the drop phase (lead)

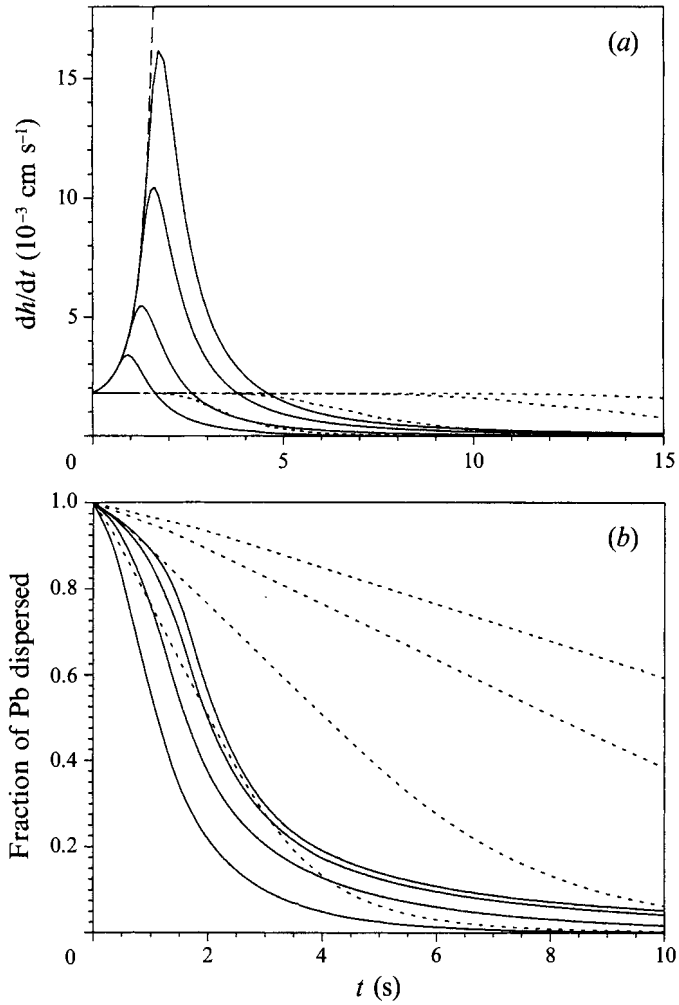

FIGURE 12. (*a*) The phase separation rate and (*b*) the fraction of lead which remains dispersed versus time for lead drops in an aluminium melt in a container of finite depth for an initial distribution having $a_o = 10$ μm, $\sigma = 2.0$ μm, $\phi_o = 0.01$. The solid curves represent $N_\tau = 5$, 10, 20 and 30, respectively, from left to right. The dotted curves in (*a*) and (*b*) are the corresponding results for containers of the same height in the absence of coalescence ($N_\tau = 0$); the dashed curve in (*a*) is the result for a semi-infinite container.

is heavier than the continuous phase, a layer of lead liquid will accumulate at the bottom of the container. Calculated collision efficiencies versus the radius of the larger drop, with van der Waals forces included, are presented for this system in figure 11 for different size ratios, following the techniques of Zhang & Davis (1991).

The phase separation velocity for an Al–Pb system with $a_o = 10$ μm, $\sigma = 2.0$ μm, and $\phi_o = 0.01$ is shown in figure 12(*a*) for different N_τ. The collision time scale, τ_c, is 0.96 s for this system. The container height, H, was varied to achieve different values of N_τ. The corresponding container heights are 0.67, 1.33, 2.67 and 4.0 cm, respectively, for $N_\tau = 5$, 10, 20 and 30. The corresponding results for containers of the same heights in the absence of coalescence are given as the dotted curves. It is apparent from these plots that coalescence significantly increases the phase separation velocity. The dashed line is the result of the phase separation velocity corresponding to a semi-infinite

container. It is seen that the initial phase separation velocities for $N_\tau = 5$, 10, 20 and 30 are the same as for the semi-infinite container. The phase separation rate then increases for short times, because coalescence leads to larger drops. Once the larger drops settle out of the dispersion, the phase separation decreases as smaller and fewer drops remain. The times at which the phase separation rate reaches its maximum are 0.9, 1.3, 1.6 and 1.7 s, for time-scale ratios $N_\tau = 10$, 20, 30 and 50, respectively. It is also shown that the maximum phase separation rate increases with increasing values of N_τ. Figure 12(*b*) shows the corresponding results for the fraction of the lead phase remaining dispersed as a function of time for the same dispersions as in figure 12(*a*). The dotted lines are the results for containers of the same height in the absence of coalescence. The times required for 90% of the lead drops to be removed are 2.9, 4.6, 5.8 and 6.2 s for $N_\tau = 5$, 10, 20 and 30, respectively. The times required for 90% of the lead drops to be removed for containers with the same heights but in the absence of coalescence are 4.3, 8.6, 17.3 and 25.9 s, respectively.

5. Concluding remarks

Quantitative predictions of the temporal and spatial evolutions of the drop size distributions and macroscopic phase separation rates in dilute droplet dispersions due to buoyancy-driven motion with coalescence are presented in this paper. Complete pairwise hydrodynamic interactions between two spherical drops are included in the analysis of the coalescence rates, but the effects of hydrodynamic interactions on the average drop velocities are neglected; this approach is valid for dispersions in which the droplet phase is a few percent by volume, or less. It is assumed that the drops have clean and uncharged interfaces, so that internal circulation occurs and there is no electrostatic repulsion. It is also assumed that the drops are sufficiently small that inertia is negligible, but not so small that Brownian motion is significant. Criteria for these restrictions have been presented previously (Zhang & Davis 1991); in general they are met for drops with diameters in the range of 2–100 μm, with the range depending weakly on the system parameters.

A dimensionless parameter, N_τ, is defined as the ratio of the characteristic sedimentation time scale to the characteristic coalescence time scale. For $N_\tau \to 0$, coalescence effects can be neglected; an analytical solution for the drop size distribution is available for this case. For $N_\tau \to \infty$, spatial variations in the population dynamics equation can be neglected, and the evolution of drop size distribution for this case has been studied in detail by Wang & Davis (1993). For finite N_τ, however, droplet coalescence will significantly increase the phase separation rate initially, and then the phase separation rate decreases after the larger drops are removed from the dispersion.

This work was supported by NASA grants NAG3-993, NAG3-1277, and NAG3-1389, and by NSF grant CTS-8914236.

REFERENCES

BERRY, E. X. & REINHARDT, R. L. 1974 An analysis of cloud drop growth by collection: Part I. Double distributions. *J. Atmos. Sci.* **31**, 1814–1824.

CLARK, T. L. 1973 Numerical modeling of the dynamics and microphysics of warm cumulus convection. *J. Atmos. Sci.* **30**, 857–878.

CLARK, T. L. & HALL, W. D. 1979 A numerical experiment on stochastic condensation theory. *J. Atmos. Sci.* **36**, 470–483.

CROWLEY, W. P. 1968 Numerical advection experiments. *Mon. Weather Rev.* **96**, 1–11.

DAVIS, R. H. & ACRIVOS, A. 1985 Sedimentation of noncolloidal particles at low Reynolds numbers. *Ann. Rev. Fluid Mech.* **17**, 91–118.

DAVIS, R. H., SCHONBERG, J. A. & RALLISON, J. M. 1989 The lubrication force between two viscous drops. *Phys. Fluids* A **1**, 77–81.

FLETCHER, C. A. J. 1991 *Computational Techniques for Fluid Dynamics 1: Fundamentals and General Techniques*. Springer.

HADAMARD, J. S. 1911 Mouvement permenent lent d'une sphere liquide et visqueuse dans un liquide visqueux. *C. R. Acad. Sci. Paris* **152**, 1735.

HALL, W. D. 1980 A detailed microphysical model within a two-dimensional dynamic framework: Model description and preliminary results. *J. Atmos. Sci.* **37**, 2486–2507.

LAX, P. D. & WENDROFF, B. 1960 Systems of conservation laws. *Commun. Pure Appl. Maths* **13**, 217–237.

PARSEGIAN, V. A. & WEISS, G. H. 1981 Spectroscopic parameters for computation of van der Waals forces. *J. Colloid Interface Sci.* **81**, 285–289.

REDDY, S. R., MELIK, D. H. & FOGLER, H. S. 1981 Emulsion stability-theoretical studies on simultaneous flocculation and creaming. *J. Colloid Interface Sci.* **82**, 116–127.

ROGERS, J. R. & DAVIS, R. H. 1990*a* Modeling of collision and coalescence of droplets in microgravity processing of Zn–Bi immiscible alloys. *Metall. Trans* **21A**, 59–98.

ROGERS, J. R. & DAVIS, R. H. 1990*b* The effects of van der Waals attractions on cloud growth by coalescence. *J. Atmos. Sci.* **47**, 1075–1080.

RYBCZYNSKI, W. 1911 Uber die fortschreitende bewegung einer flussigen kugel in einem zahen medium. *Bull. Acad. Sci. Cracovie* **A**, 40.

SATRAPE, J. V. 1992 Interactions and collisions of bubbles in thermocapillary motion. *Phys. Fluids* A **4**, 1883–1900.

SMITHELLS, C. J. 1962 *Metals-Reference Book*, p. 698. Butterworths.

WANG, H. & DAVIS, R. H. 1993 Droplet growth due to Brownian, gravitational, or thermocapillary motion and coalescence in dilute dispersions. *J. Colloid Interface Sci.* **159**, 108–118.

ZHANG, X. & DAVIS, R. H. 1991 The rate of collisions due to Brownian or gravitational motion of small drops. *J. Fluid Mech.* **230**, 479–504.

ZHANG, X., WANG, H. & DAVIS, R. H. 1993 Collective effects of temperature gradients and gravity on droplet coalescence. *Phys. Fluids* A **5**, 1602–1613.